ADVANCED MATERIALS TECHNOLOGIES
www.advmattechnol.de

# Flytrap Inspired pH-Driven 3D Hydrogel Actuator by Femtosecond Laser Microfabrication

*Jian-Yu Wang, Feng Jin,* Xian-Zi Dong, Jie Liu, and Mei-Ling Zheng**

**With the development of bionics and nanophotonics, hydrogel microactuators capable of responding to external stimuli to produce controllable deformations have attracted a great deal of interest. These microactuators hold significant promise in areas such as bionic devices, soft robotics, and precision sensors. It is not a trivial task to make such small devices as well as to make them work in a controlled manner. Here, inspired by the intelligent response of flytrap, a smart hydrogel microactuator based on a bionic asymmetric structure is demonstrated. The designed asymmetric microstructure is fabricated by femtosecond laser direct writing with deformation time of 1.2 s and recovery time of 0.3 s. The grasping and releasing behavior of the microactuator for micro-objects can be realized and tuned by using pH-triggered shape changes, demonstrating its potential for applications, such as flexible robotics, smart sensors, and microscopic manipulation.**

## 1. Introduction

Stimuli-responsive behaviors of plants and animals have been critical to their survival and reproduction throughout millions of years of evolution.[1,2] Inspired by nature, intelligent manipulation actuators based on stimuli responsive behavior have been widely studied and applied in soft robotics, aerospace engineering, flexible electronics, biomedical, etc.[3–6] Recently, research on asymmetric stimuli response have been rapidly developed due to the programmability and manipulability of asymmetric structures.[7–9] Liu et al. mimic the movement of eagle claws and tendrils climbing plants to create programmable asymmetric GO/polymer bilayer actuators for controlled object transport through precise local responses.[10] Inspired by the opening and closing of flower petals, Zhang et al. achieved bionic dual 3D laser printing by programmatically tuning the cross-linked network density of nanoscale hydrogels.[11] Further, Soh et al. used an asymmetric stimulus response to link the concepts of materials and mathematics, giving the hydrogel the ability to handle time derivatives.[12] These asymmetric actuators can be driven by external stimuli, such as light, temperature, pH, and magnetic fields to produce on-demand deformation with specific functions.[13–16] For the construction of the asymmetric actuators, the general fabrication methods include UV-assisted printing, fused deposition modeling (FDM), femtosecond laser direct writing (FsLDW), etc.[17–20] Nowadays, 4D printing of asymmetric actuators by combining 3D printing with stimulus-responsive materials is used in soft robotics, biomedical devices, and energy harvesting systems due to the advantages of large amplitude and complex response.[21–25]

Notably, flytrap is an interesting plant with the capability to capture small insects based on the fast asymmetric stimuli-responsive behaviors. When the leaf of flytrap is stimulated by external insects, the ion concentration in the cytoplasm of its sensory cells changes rapidly, resulting in rapid water loss from the cells in the center of the leaf. Due to the sudden loss of water, a pair of flytrap leaves close in a very short period of time, and accomplish the capture of insects between the leaves.[26,27] At the macroscopic scale, research on the preparation of flytrap-like structures using UV polymerization is well developed.[28–31] Priimagi et al. demonstrated a light-driven bionic flytrap structure based on light-responsive liquid crystal elastomers, which enables autonomous closure and object recognition.[32] Sui et al. prepared a double-gradient laminar structure of ultrafast actuators by combining graphene with temperature-responsive materials, inspired by the extremely fast motion of the flytrap generated by the accumulation and rapid release of elastic energy.[33] Analogous to the macroscopic scale structures, microscopic bionic flytrap actuators are of great importance for the applications in micromanipulation, microrobotics, microfluidics, biomedicine, etc.[34–42] However, the manufacturing of bionic flytrap microactuator is still challenging due to the difficulty in precisely controlling the composition and responsive property of the 3D microstructure at the microscale.

In this study, we demonstrate the smart response properties of a 4D printed asymmetric hydrogel microactuator inspired by the flytrap. The bionic microactuator was fabricated by femtosecond laser direct writing (FsLDW) of responsive photoresist. We first formulated a stimulated responsive photoresist containing 2-(dimethylamino)ethyl methacrylate (DMAEMA) for

J.-Y. Wang, F. Jin, X.-Z. Dong, J. Liu, M.-L. Zheng
Laboratory of Organic NanoPhotonics and CAS Key Laboratory of Bio-Inspired Materials and Interfacial Science
Technical Institute of Physics and Chemistry
Chinese Academy of Sciences
No. 29, Zhongguancun East Road, Beijing 100190, P. R. China
E-mail: jinfeng@mail.ipc.ac.cn; zhengmeiling@mail.ipc.ac.cn
J.-Y. Wang
School of Future Technology
University of Chinese Academy of Sciences
Yanqihu Campus
Huaibei Town, Huaibei Zhuang, Huairou District, Beijing 101407, P. R. China
The ORCID identification number(s) for the author(s) of this article can be found under https://doi.org/10.1002/admt.202200276.

DOI: 10.1002/admt.202200276

 

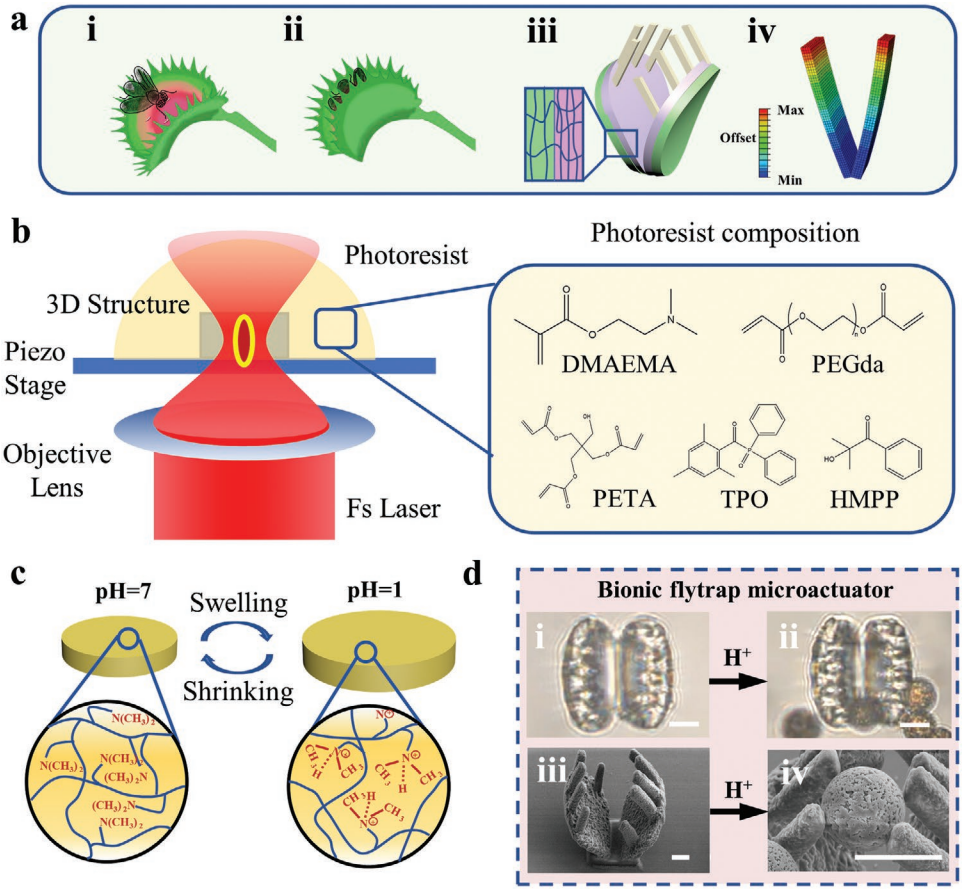


**Figure 1.** Schematic design and fabrication of the bionic hydrogel microactuator. a(i,ii) Capture behavior of the flytrap. (iii) Structural design of the bionic microactuator. Inset diagram indicates the asymmetry of the crosslinking density. (iv) Simulation of deformation behavior of the bionic microactuator. Blue to red represents the increase in offset. b) Schematic diagram of FsLDW of asymmetric bionic microactuator. The inset presents the compositions of the photoresist. c) Schematic representation of the responsive mechanism of the pH-induced deformable hydrogel. d) Bright field images of the bionic microactuator under (i). primitive condition and (ii). acidic condition. SEM images of the bionic microactuator under (iii), initial condition and (iv) acidic condition. Scale bar in d) is 10 µm.

two-photon polymerization (TPP) fabrication. The TPP properties of the responsive photoresist and the responsive properties of the obtained microstructures were investigated in detail. Controllable driving behavior is achieved by tuning fabrication parameters, such as power density, scanning path, etc., to modulate the crosslinking density of the microstructures spatially and temporally. The micrometer-sized hydrogel actuator not only exhibits fast pH response time, but also can tune the capture and release behavior of tiny target particles by adjusting the pH response strategy.

## 2. Results and Discussion

4D printing of bionic hydrogel microactuator was achieved by FsLDW of photoresists containing stimuli-responsive monomer, as shown in **Figure 1**. Flytrap is capable of catching insects by rapid shape change of the leaves when stimulated by mechanical forces (Figure 1a(i),(ii)). Inspired by flytrap, we designed an asymmetric hydrogel microactuator with a gradient crosslinking density (Figure 1a(iii)). The change in crosslinking is expected to affect the responsiveness, so that the asymmetric leaves of the microactuator drive the toothed structure to close and grasp. The deformation of the microactuator was simulated employing ABAQUS software based on a model of a double-layer asymmetric structure (Figure 1a(iv); and the Supporting information). According to the numerical simulation, the microactuator will swell anisotropically when the pH of the solution changes, resulting in the controllable responsive behaviors.

Subsequently, high-fidelity hydrogel microactuators were obtained by FsLDW. As shown in Figure 1b, the fabrication system contains an oil immersion objective lens which focuses a 780 nm femtosecond laser beam into the photoresist. The laser beam usually has a spatial Gaussian distribution and cross-linking of the material occurs only at the laser focus where the laser power is higher than the fabrication threshold. The laser scanning path is determined by a computer-controlled galvano-mirrors, yielding the designed microstructures. In order to realize responsive behavior, DMAEMA was used to formulate stimuli-responsive photoresist precursors (Figure 1b). The side chains of the obtained DMAEMA-based hydrogels contain protonatable aliphatic tertiary amine groups (Figure 1c). When exposed to an acidic solution (pH = 1), the tertiary amine

groups become positively charged due to the protonation of hydrogen ions.[43] The electrostatic repulsion between the molecular chains caused by these charges expands the size of the polymer grid and the entry of additional water molecules causes the hydrogel to increase in volume and swell. On the contrary, the addition of alkaline solution (pH = 13) will deprotonate the tertiary ammonium cations and decrease the interchain spacing, resulting in the shrinking of the hydrogel owing to the reduced volume.

Controlled deformation of the stimulated hydrogel microstructure can be achieved by adjusting the FsLDW parameters. Figure 1d shows an asymmetric bionic microactuator prepared by a cyclic fabrication method. This method achieves controlled crosslinking densities on the inner and outer sides of the blade structure to achieve asymmetry, facilitating the achievement of flytrap-like deformation behavior in an acidic environment. The closing of the microactuator caused by the acidic solution will prevent the polystyrene (PS) microspheres from flowing freely in the liquid, resulting in the capture of the PS microsphere by the microactuator is completed.

The polymerization properties of hydrogel photoresists were studied as shown in **Figure 2**. Figure 2a; and Figure S1 (Supporting Information) show that the solution of the monomer mixture does not exhibit obvious absorption in the wavelength range of 300–800 nm, while diphenyl(2,4,6-trimethylbenzoyl) phosphine Oxide (TPO) and 2-hydroxy-2-methylpropiophenone (HMPP) as photoinitiator show absorption peaks at 380 and 330 nm. After the addition of photoinitiator, a clear absorption band appears at 330–380 nm, while there is no absorption at 780 nm. Two-photon polymerization may occur in the photoresist by the irradiation of 780 nm femtosecond laser. To determine the optical nonlinear absorption process during the FsLDW of the photoresist, the dependence of the threshold power density $P_{th}$ on the scanning speed $V_s$ was investigated. Figure 2b demonstrates that the laser threshold power for the photoresist with different initiator contents varied between 86.6 and 252.2 GW cm$^{-2}$. There is a clear regularity of the laser threshold power density with respect to the scanning speed, which can be described using specific functions to determine the mechanism of the polymerization reaction.[44] For higher scanning speeds ($V_s \geq 50$ µm s$^{-1}$)

$$P_{th} \propto C \times V_s^{1/N} \quad (1)$$

where $N$ is the nonlinear index of the photoinitiator and $C$ is a constant related to the fabrication properties of the photoresist. Figure 2b illustrates that the value of $N$ varies between 1.95 and 2.08, which are close to the two-photon absorption coefficient as the initiator content varies. It is also known that the low-speed scanning will deviate from the fitted value due to the presence of oxygen that quenches the radicals.[45] Therefore, the power density used at low scanning speeds must be slightly higher to produce enough radicals for the reaction to continue. To minimize the possible effect of residual initiator on the microstructures, a photoresist with initiator content of 1 wt% was used for the fabrication of the hydrogel microstructures. As shown in Figure 2c, concentric ring structures were fabricated with different power density to investigate the effect of power density

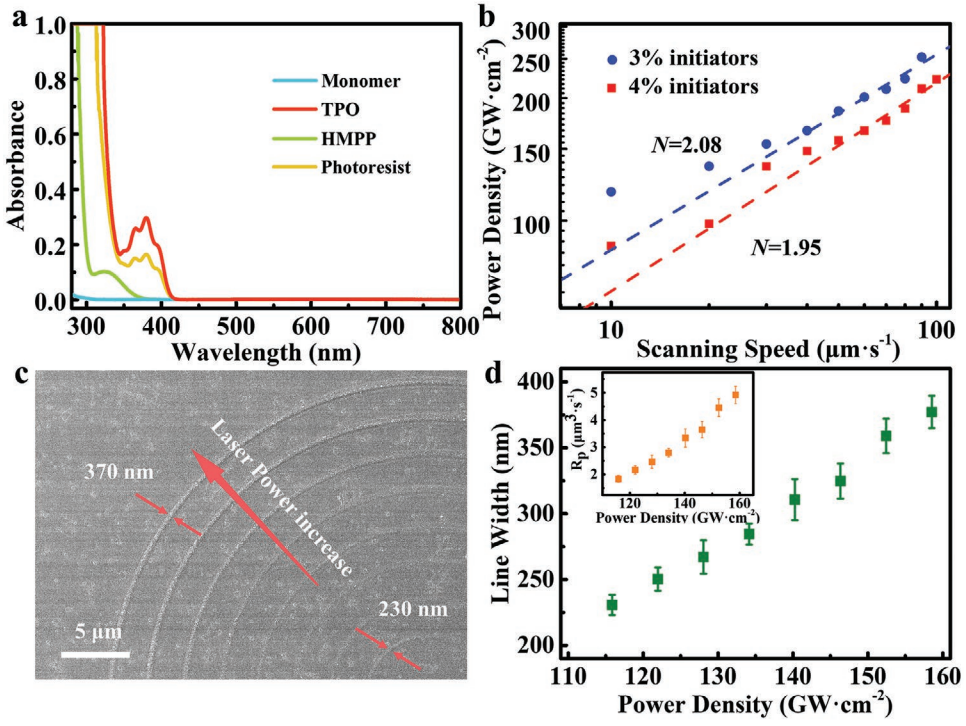


**Figure 2.** a) UV–vis absorption spectra of TPO, HMPP, monomer mixture, and photoresist ethanol solutions. b) The dependence of laser threshold power density on scanning speed at different initiator contents. c) SEM image of polymer line fabricated by FsLDW. The minimum line width is 230 nm, which was fabricated with a power density of 116 GW cm$^{-2}$. d) The influence of power density on polymerized hydrogel linewidth. The inset is the influence of the power density on polymerization rate of the hydrogel.

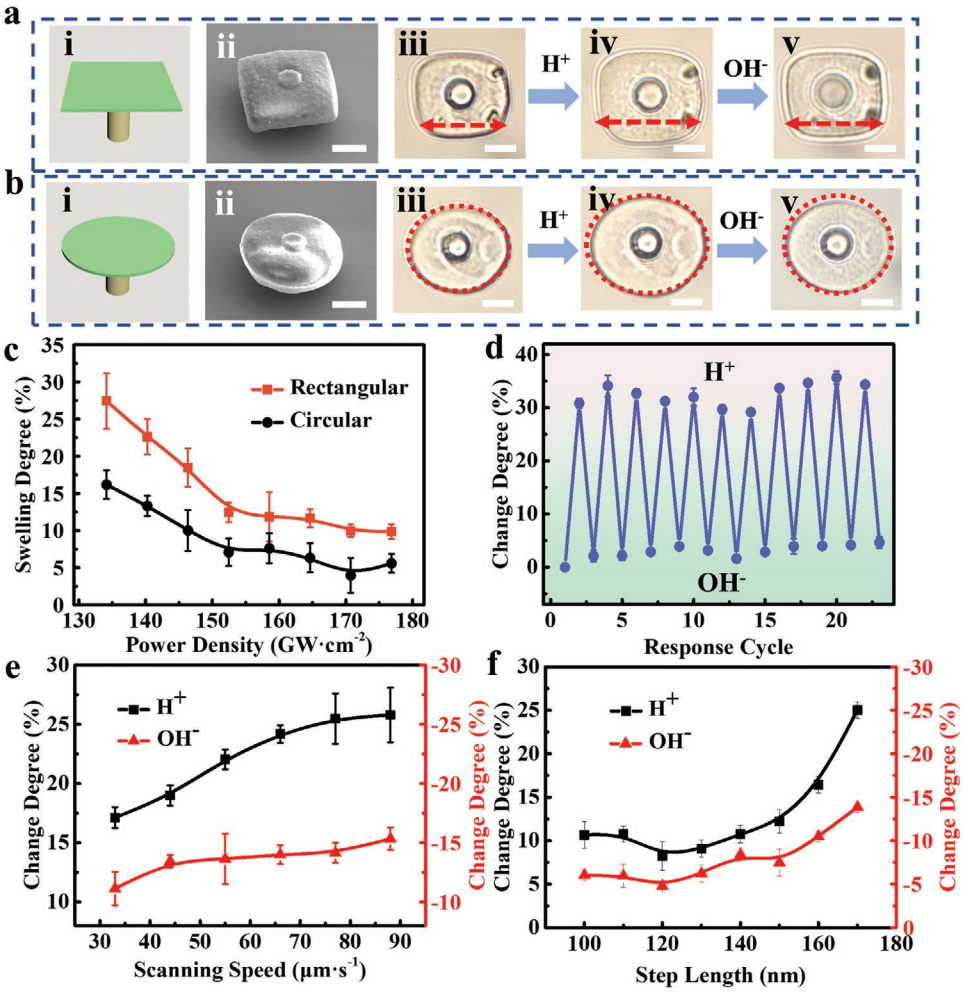


**Figure 3.** Stimuli-responsive properties of the symmetric hydrogel microstructures fabricated by FsLDW. a(i). Model diagram, and (ii). SEM image of the rectangular hydrogel microstructure. (iii–v). Bright field images of the rectangular microstructures at different pH. b(i) Model diagram, and (ii). SEM image of the circular hydrogel microstructure. (iii–v). Bright field images of circular structures at different pH. c) The influence of the power density on the swelling degree of the hydrogel microstructures under different pH. d) Reversible swelling behaviors of the rectangular hydrogel microstructures. e) The influence of the scanning speed on the change degree of the hydrogel microstructures. f) The influence of the step length on the change degree of the hydrogel microstructures. Scale bar is 10 μm.

on the linewidth. The statistical results (Figure 2d) illustrate that the resolution of the photoresist can be improved to 230 nm at a power density of 116 GW $cm^{-2}$, and the linear structures can be stably fabricated in the laser power range of 116–159 GW $cm^{-2}$. The polymerization rate $R_p$ of FsLDW can be calculated by[46]

$$R_p = \pi \times (d/2)^2 \times V_s \quad (2)$$

where $d$ represents the line width and $V_s$ represents the scanning speed. The inset of Figure 2d shows that the polymerization rate can be tuned between 3.14 and 11.2 $\mu m^3\ s^{-1}$. The results imply that high-precision microstructures can be achieved by tuning the power density.

To evaluate the responsive property of the hydrogel microstructures by FsLDW, the reversible swelling and shrinking behaviors were investigated under different pH conditions as shown in **Figure 3**. In terms of design, suspended microstructures are anchored on cylindrical stages with 8 μm height to prevent contact between the microstructure and the substrate. As shown in the scanning electron microscope (SEM) images of Figure 3a(ii),b(ii), the microstructures are identical to the designed model with no apparent adhesion of the bottom to the substrate. With the injection of acidic solution, once the pH of surrounding is lower than the $pK_a$ of the DMAEMA-based hydrogel, the protonation will cause hydrogel to exhibit the swelling behavior. This behavior can be reversibly changed by shifting the pH of the solution. Subsequently, with the addition of alkaline solution, the deprotonation effect makes the polymer chain spacing shorter and the structure can be recovered to the initial state. Different fabrication parameters were used to investigate the effect of crosslinking density on the pH responsive of hydrogel microstructures. *Cd* (change degree of the size) was introduced to quantify this effect.

$$Cd = \frac{S_{after} - S_{before}}{S_{before}} \quad (3)$$

Here, $S_{before}$ is the area of the preresponse microstructure and $S_{after}$ is the area of the postresponse microstructure. As shown in Figure 3c, when the power density is increased from 134 to 177 GW cm$^{-2}$ (with the scanning speed of 44 μm s$^{-1}$ and the step length of 160 nm), *Cd* of the rectangular structure decreases from 27% to 10%. The maximum swelling can be obtained when the power density is 134 GW cm$^{-2}$. The reason for this is that higher power density increases the crosslinking density, which brings about a decrease in the responsive capability of the microstructure.[47] Therefore, it is feasible to obtain hydrogel microstructures with different responsiveness by varying the power density. We verified the reversibility of the fabricated hydrogel microstructures by multiple cycles of swelling experiments. Figure 3d shows that there is no obvious degradation of the responsiveness of the microstructure even after 23 cycles. In addition to the power density, scanning speed, and step length can also be adjusted to control the responsive property of the hydrogel microstructures (Figure S2, Supporting Information). Figure 3e,f depict the influence of scanning speed and step length on the response. Higher scanning speeds or larger step lengths result in a lower crosslinking density of the hydrogel microstructure, leading to an enhanced responsiveness.

In order to achieve fine and diverse drives, asymmetric microstructures with controlled crosslinking density are required. From the previous discussion, the responsiveness of the hydrogel microstructures can be directly adjusted by the laser parameters. It is expected that the gradient crosslinking density resulting from FsLDW cyclic fabrication can enable controllable driving of microstructures (**Figure 4**a(i); and Figure S3, Supporting Information). Figure 4a(ii) shows that the asymmetric microarm in the simulation can bend toward the lower responsive side where the crosslinking density is higher when the response occurs. By using confocal fluorescence microscopy, the shape change of the microarm under acid treatment was confirmed, as shown in Figure 4a(iii). Autofluorescence of the microarm was observed, while excited by 488 nm irradiation and recorded between 490 and 540 nm. The asymmetric microarm can bend in a specific direction after the addition of acidic solution, agreeing with the simulation result.

We further investigated the influence of laser parameters including power density and scanning speed on the responsive property of the asymmetric microstructures. As shown in Figure 4b, power density was varied to construct a series of hydrogel microarms. Slight bending of the hydrogel microarm in the development process was observed due to the gradient crosslinking density, similar to the previous report.[48] Tilted SEM image (Figure 4b, inset) indicates that the microarms are not adhered to the substrate but suspended in the air. There are two sets of microarms with different laser parameters shown

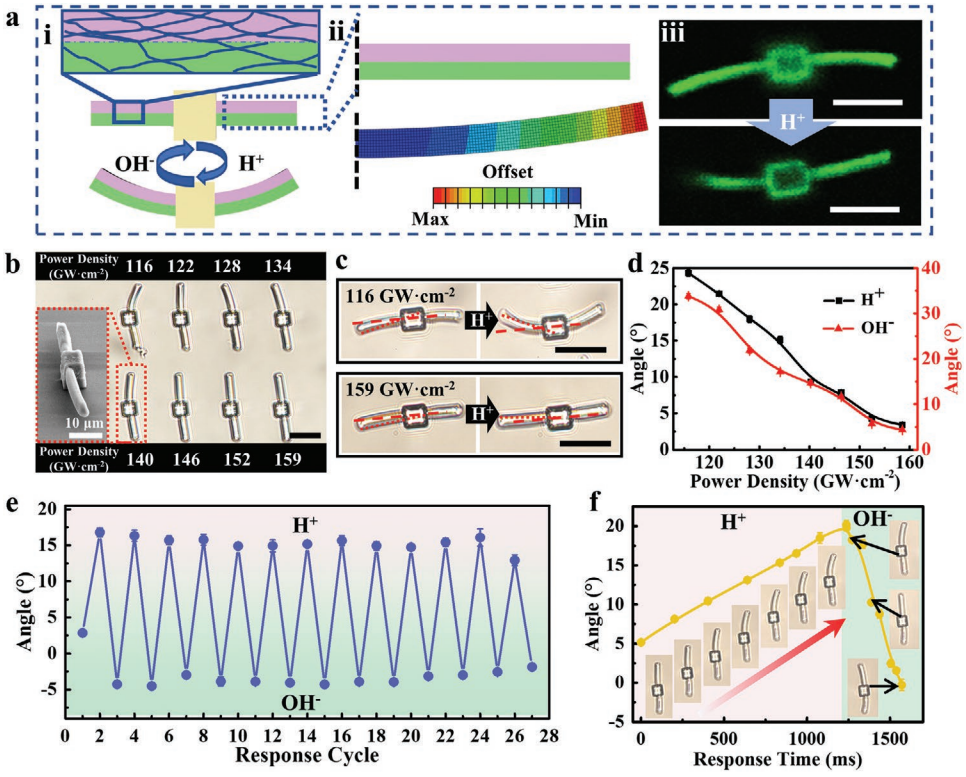


**Figure 4.** Responsive property of the asymmetric hydrogel microarms fabricated by FsLDW. a(i) Schematic diagram of the pH-responsible asymmetric microarm. (ii) Simulation of pH-induced shape change of the asymmetric hydrogel microarm using commercial FEA software. (iii) Confocal fluorescence microscopy images of the hydrogel microarm under acid treatment. b) Bright field images of asymmetric microarms fabricated with different laser powers. The inset shows the SEM image of the microarm fabricated with power density of 140 GW cm$^{-2}$. c) Response of the asymmetric microarm fabricated with different power density. d) Bending angle variation of asymmetric microarms fabricated with different power density under acid and alkali treatment. e) Reversible bending behavior of asymmetric hydrogel microarms. f) Response time of asymmetric hydrogel microstructure under different environments. Scale bar is 20 μm.

here in Figure 4c for comparison of the responsive behavior. When the power density increases from 116 to 159 GW cm$^{-2}$, the bending angle of the asymmetric hydrogel microarm decreases from 20° to 5°. The decrease of bending angle is attributed to the increased crosslinking intensity of the low crosslinking portion, resulting in the dropped asymmetry of the microarms. Similar to the effect of power density, the increase of scanning speed increases the bending angle of the microarm as shown in Figure S4c (Supporting Information). However, an appropriate scanning speed is important as incomplete structures do not exhibit bending behavior through high scanning speeds, as shown in the red dashed line in Figure S4a (Supporting Information).

Reliable and effective microactuator requires fast and stable responsive behavior. To confirm the reversibility of the response process, the samples were characterized for 26 cycles and the amount of shape change was counted for each time. As shown in Figure 4e, the responsiveness of the structure did not change noticeably with increasing number of cycles, showing good reversibility and stability. In addition to the degree of responsiveness, the response time is also an important characteristic of the microstructure. For a typical asymmetric microarm ($P$ = 134 GW cm$^{-2}$, $V$ = 44 μm s$^{-1}$), the change in bending angle from 5° to 15° during bending can be completed rapidly in 1.2 s and the recovery process can be completed within 0.3 s (Figure 4f). The asymmetric structure obtained by tuning the fabrication parameters of FsLDW has excellent stability and cycling reliability. The reliable and fast response endows the asymmetric hydrogel microstructures potential for the applications in smart microactuators.

Bionic hydrogel microactuators were designed, fabricated, and studied after achieving controllable structural deformation of the asymmetric hydrogel microstructures. **Figure 5**a(i) shows the bionic flytrap model designed by using 3Ds Max software. By converting the model through programming algorithm, the files can be obtained to fabricate the designed microstructure. The detailed structural parameters of the microactuator are shown in Figure S5 (Supporting Information). Bright field image and SEM image (Figure 5a(ii),(iii)) demonstrate that the microactuator can be obtained by FsLDW with good fidelity. Finite element analysis software was used to investigate the shape change of the hydrogel microactuator when exposed to acidic solution. The bending direction of the simulation results (Figure 5a(iv)) is consistent with the design, facilitating the preparation of bionic hydrogel microactuators. Figure 5b(i) shows a schematic representation of the capture and release process of an asymmetrically deformed bionic microactuator. As the microsphere enters the microstructure, the protonation owing to the addition of the acidic solution causes the gradient cross-linked leaves structure to deform and then fold together. The deformation would lead to the closure of the toothed structure, enabling the capture of the microsphere. After capturing the microsphere, the acidic environment is neutralized by the addition of an alkaline solution (pH = 13). The deprotonation brought about by the reduced hydrogen ion content returns the structure to its original shape, the opening in the microactuator becomes larger and the trapped microsphere can be released by the action of the liquid. The fabricated hydrogel microactuator is used in an aqueous phase environment. Therefore, the temperature limit at which this hydrogel microactuator can be used is 0–100 °C. This is the temperature range in which water remains in a liquid state. The bright field images in Figure 5b(ii–v) show the capture and release of the microsphere by the bionic microactuator. The microactuator has an opening size of 12.5 μm in the original state, which is reduced to 7 μm by the addition of the acidic solution (Figure S6, Supporting Information). Therefore, the bionic hydrogel microactuator can capture microspheres with proper size (e.g., PS microspheres of 10 μm in diameter). The SEM images shown in Figure 5c confirm that the PS microspheres can be captured

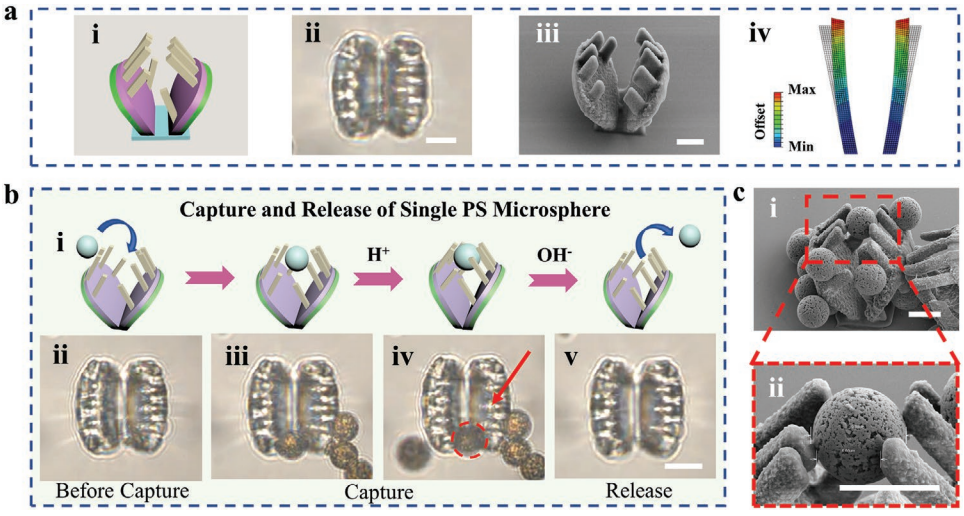


**Figure 5.** On-demand response of the bionic hydrogel microactuator fabricated by FsLDW. a(i) 3Ds max model, (ii) bright field image, and (iii) SEM image of the bionic flytrap microstructure. (iv) Simulation of the pH response of the bionic flytrap microstructure. b(i) Schematic diagram of the microsphere capture and release behavior of the bionic hydrogel microactuator. (ii) Bright field image of the bionic microstructure before the capture behavior. (iii,iv) Bright field images of the bionic microstructure with captured PS microsphere. (v) Bright field image of the bionic microstructure after the release behavior. c(i) SEM image and (ii) magnified SEM image of the hydrogel microstructure with captured microsphere. Scale bar is 10 μm.

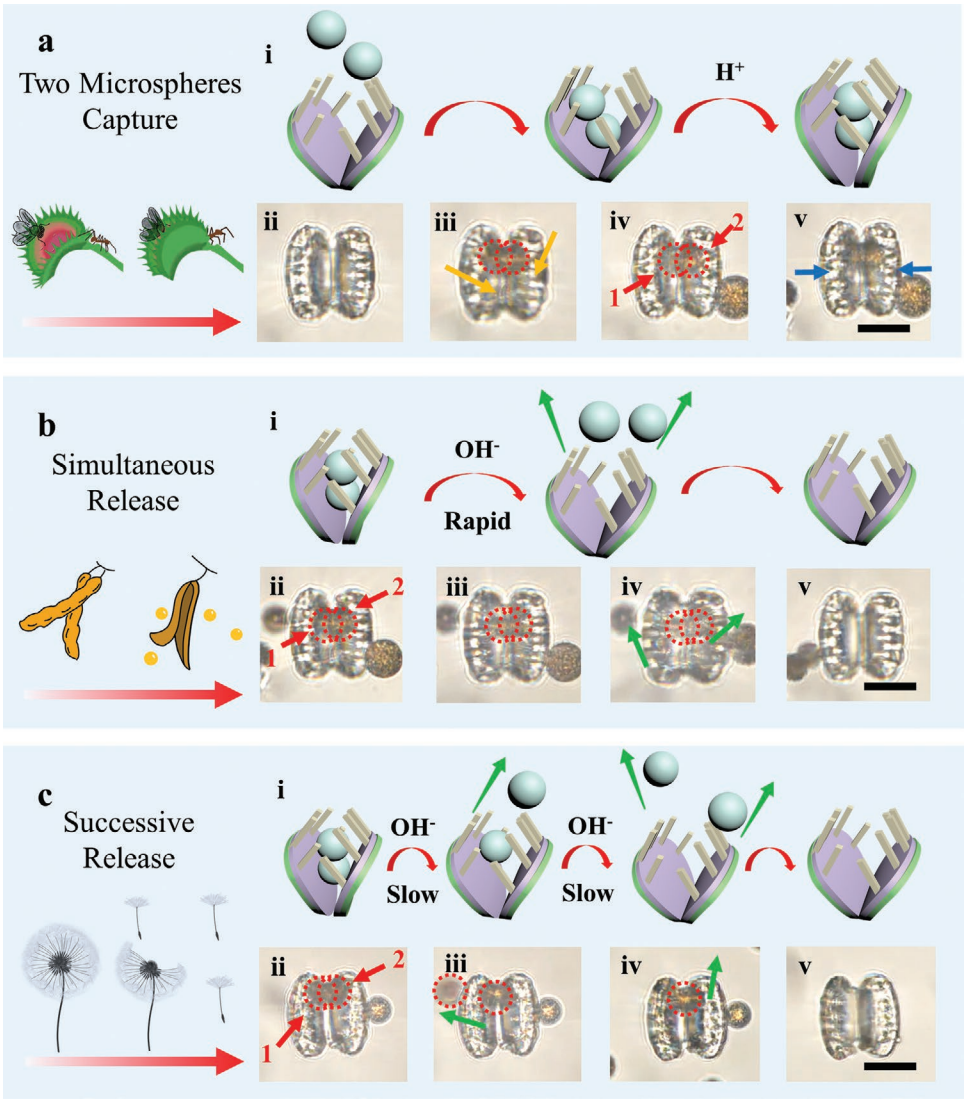


**Figure 6.** Capture and release behaviors of multiple PS microspheres by the bionic flytrap microactuators. a(i) Schematic diagram of two PS microsphere capture behaviors. (ii–v) Bright field images of two PS microspheres captured by the bionic flytrap microactuator. b(i) Schematic diagram of the simultaneous release of two PS microspheres by the bionic flytrap microactuator. (ii–v) Bright field images of the simultaneous release process of two PS microspheres by the bionic flytrap microactuator. c(i) Schematic diagram of the successive release behavior of two PS microspheres by the bionic flytrap microactuator. (ii–v) Bright field images of successive release process of two PS microspheres by the bionic flytrap microactuator. Scale bar is 25 μm.

by the toothed structure of the bionic hydrogel microactuator. The controlled manipulation behavior of the bionic hydrogel microactuator has potential applications in micromanipulation and soft robotics.

Moreover, we depict the controllable capture and release behavior of the bionic microactuator for two PS microspheres. The bright field images in **Figure 6**a demonstrate the capture of two PS microspheres by the bionic flytrap microactuator. The capture behavior of two PS microspheres is similar to that of single PS microsphere. After two PS microspheres were observed to flow into the microactuator, an acidic solution (pH = 1) was added immediately. The protonation caused by the hydrogen ions from the acidic solution causes the asymmetric microstructure to close and achieve the trapping behavior.

The release behaviors of the captured two PS microspheres by the bionic microactuator can be precisely tuned by controlling the speed for the addition of alkaline solution. Addition of the acidic solution brings about a change in the shape of the microactuator along with the accumulation of elastic energy. The elastic energy is temporarily stored through reversible ionic interactions within the polymer. When the external environment changes, the microactuator will undergo a change from a higher to a lower state of elastic energy and will release the elastic energy as kinetic energy.[49] Therefore, it is possible to modulate the release behavior by regulating the duration of the stimuli responsive process. As shown in Figure 6b; and Movie 2 (Supporting Information), if the acidic solution is completely removed from the environment and an alkaline solution

(pH = 13) is immediately added, the rapid change in the solution environment will cause the elastic potential energy accumulated by the microactuator to be released in a short period of time. Thus, the internal PS microspheres will be released from the structure simultaneously under the kinetic energy generated by the deformation and the liquid flow. This is similar to the seed transmission behavior of the seeds of plant pods.[50] By contrast, if an alkaline solution (pH = 13) is slowly added to the acidic environment after the trapping behavior, a longer acid-base neutralization reaction occurs slowly, and the pH gradually increases. As shown in Figure 6c; and Movie 3 (Supporting Information), the prolongation of response time under the same response degree will lead to a decrease in the power of elastic energy release. Therefore, the release of PS microspheres from the bionic microactuator is relatively slow. The internal PS microspheres are negligibly affected by the kinetic energy generated by the deformation and moved only by the flow of the liquid. Just as the seeds of a dandelion move gradually with the wind, the gentle release leads to a successive release of the PS microspheres. This difference in release behavior increases the manipulability of the microactuator for micro-objects.

## 3. Conclusion

In conclusion, stimuli-responsive bionic asymmetric microactuators were prepared by femtosecond laser two-photon polymerization fabrication. FsLDW was used to fabricate photoresists containing pH responsive monomer DMAEMA. The tuning of fabrication parameters enables the manufacture of hydrogel microstructures with designed local crosslinking density, resulting in the controllable responsive behaviors of the hydrogel microstructures. The response time of this asymmetric structures can be controlled within 1.2 s, while the recovery process can be completed within 0.3 s. Based on pH-induced asymmetric deformation, the designed flytrap-like structure allows for the capture of single microsphere as well as multiple microspheres. Moreover, the release behavior of multiple microspheres can be precisely manipulated by employing different release strategies, thus enabling simultaneous release processes and successive release processes. The controlled manipulation of the bionic microactuator in this study will increase the potential for precise capture and release of microobjects, enabling the preparation of smart hydrogel devices. This has potential applications in research areas, such as soft-body robotics, microsensors, and Micro Electro Mechanical Systems (MEMS).

## 4. Experimental Section

*Chemicals and Materials*: TPO was purchased from Shanghai Shaoyuan Co. Ltd., HMPP, and glycerol was purchased from J&K Chemical Co. Ltd., Pentaerythritol triacrylate (PETA) was purchased from Kyoeisha Chemical Co. Ltd., poly (ethylene glycol) diacrylate (PEGda, $M_w \approx 700$) was purchased from Sigama-Aldrich, 2-(dimethylamino)ethyl Methacrylate (DMAEMA) was purchased from Tokyo Chemical Industry Co. Ltd. 3-(Trimethoxysilyl) propyl methacrylate (KH-570) was purchased from Nanjing Chuangshi Chemical Co. Ltd., Ethanol, hydrochloric acid (HCl) and sodium hydroxide (NaOH) were purchased from Modern Oriental (Beijing) Technology Development Co. Ltd. The cover glass was purchased from Yancheng Flying Boat Glass Co. Ltd. All the chemicals are used without further purification.

*Preparation of Photoresist*: To prepare pH-responsive hydrogel photoresist, the component of the photoresist according to macroscopic hydrogel response experiments (Figures S7 and S8, Supporting Information) was optimized. To make the optimized photoresist, TPO (0.01 g) and HMPP (0.01 g) as photoinitiator were added to DMAEMA (0.15 g), PETA (0.3 g), and PEGda (0.53 g). Glycerol (0.1 g) was added to the mixture as thickener and stirred overnight. The photoresist was placed in dark for 48 h. Finally, the photoresist was transferred to a brown glass vial and stored away from light.

*Substrate Functionalization*: Place the rectangular glass coverslips in deionized water with detergent for 30 min of ultrasonic cleaning. The glass coverslips were cleaned by ultrasonic in deionized water for six times and then dried in an oven. The dried glass coverslips were immersed in 5 wt% KH-570/toluene solution for 2 h. Then, the glass coverslips were washed quickly with anhydrous ethanol and dried.

*Fabrication of Hydrogel Microstructures*: As shown in Figure S9 (Supporting Information), the fabrication system consists of a femtosecond laser (ErFemto-780 ProH), a galvano-mirrors (SCANLAB, HurrySCAN 14), a piezostage (PI, P-622.ZCL), a ND filter and a computer. The femtosecond laser pulse has a central wavelength of 780 nm, a pulse duration of 150 fs and a repetition frequency of 100 MHz. The mechanical shutter is used to control the exposure time. And the ND filter is used to regulate the power of the femtosecond laser for fabricating microstructures. The fabrication procedure is shown in Figure S10 (Supporting Information). The laser beam is focused into the photoresist through a 60 × oil immersion objective lens with a high numerical aperture (*N.A.*) of 1.42, which will produce a beam spot with a diameter of 388 nm. The path of the laser beam is controlled by a galvano-mirrors, which is then scanned to fabricate layer by layer using a computer predesigned program. The hydrogel microstructures are obtained after developing process.

*Characterization*: UV–vis spectra were taken by a Shimadzu UV-2550 spectrophotometer. The concentration of the monomer ethanol solution was 0.02 g $mL^{-1}$, the concentration of initiator ethanol solution was $9 \times 10^{-3}$ g $mL^{-1}$, and the concentration of photoresist ethanol solution with 1 wt% initiators was 0.5 g $mL^{-1}$. SEM images were measured by a field emission scanning electron microscope (FESEM, Hitachi S-4800). CCD DS-Ri2 (Nikon, Japan) adapted in Nikon Eclipse Ti-E microscope along with a 50 × objective lens (*N.A.* = 0.8) was used to record the response process. The DS-Ri2 is able to obtain 30 fps video at 1636 × 1088 pixels. The bending behavior was obtained by continuously recording the response process. The bending angle of the asymmetric microarm in each frame of the experimental results was measured. Then the bending angle was determined by averaging 10 independent measurements. pH response experiments were performed using HCl solution (pH = 1) and NaOH solution (pH = 13). For confocal fluorescence microscopy, a 488 nm laser with a power of 2.5 mW was used.

## Supporting Information

Supporting Information is available from the Wiley Online Library or from the author.

## Acknowledgements

The authors were grateful for the financial support of the National Key R&D Program of China (Grant Nos. 2016YFA0200501 and 2016YFC1100502), the National Natural Science Foundation of China (NSFC, Grant Nos. 51673208, 51473176, 61975213, and 51901234), Beijing Natural Science Foundation (Grant No. 2182079), Cooperative R&D Projects between Austria, FFG and China, CAS (No. GJHZ1720), and

 

International Partnership Program of Chinese Academy of Sciences (No. GJHZ2021130).

## Conflict of Interest

The authors declare no conflict of interest.

## Data Availability Statement

The data that support the findings of this study are available from the corresponding author upon reasonable request.

## Keywords

4D Printing, biomimetic microstructure, femtosecond laser, photoresist, stimuli-responsive hydrogel, two-photon polymerization

Received: February 20, 2022
Revised: March 8, 2022
Published online:

[1] Y. S. Zhang, A. Khademhosseini, *Science* **2017**, *356*, eaaf3627.
[2] C. Kaspar, B. J. Ravoo, W. G. van der Wiel, S. V. Wegner, W. H. P. Pernice, *Nature* **2021**, *594*, 345.
[3] H. Kim, S.-k. Ahn, D. M. Mackie, J. Kwon, S. H. Kim, C. Choi, Y. H. Moon, H. B. Lee, S. H. Ko, *Mater. Today* **2020**, *41*, 243.
[4] M. Li, A. Pal, A. Aghakhani, A. Pena-Francesch, M. Sitti, *Nat. Rev. Mater.* **2022**, *7*, 235.
[5] M. A. English, L. R. Soenksen, R. V. Gayet, H. d. Puig, N. M. Angenent-Mari, A. S. Mao, P. Q. Nguyen, J. J. Collins, *Science* **2019**, *365*, 780.
[6] S. Li, H. Bai, Z. Liu, X. Zhang, C. Huang, L. W. Wiesner, M. Silberstein, R. F. Shepherd, *Sci. Adv.* **2021**, *7*, eabg3677.
[7] P. Illien, R. Golestanian, A. Sen, *Chem. Soc. Rev.* **2017**, *46*, 5508.
[8] Z. Li, P. Liu, X. Ji, J. Gong, Y. Hu, W. Wu, X. Wang, H.-Q. Peng, R. T. K. Kwok, J. W. Y. Lam, J. Lu, B. Z. Tang, *Adv. Mater.* **2020**, *32*, 1906493.
[9] K. Wang, J. Ren, S. Yang, H. Wang, *Adv. Mater. Technol.* **2021**, *6*, 2100158.
[10] Y. Dong, J. Wang, X. Guo, S. Yang, M. O. Ozen, P. Chen, X. Liu, W. Du, F. Xiao, U. Demirci, B.-F. Liu, *Nat. Commun.* **2019**, *10*, 4087.
[11] Y.-L. Zhang, Y. Tian, H. Wang, Z.-C. Ma, D.-D. Han, L.-G. Niu, Q.-D. Chen, H.-B. Sun, *ACS Nano* **2019**, *13*, 4041.
[12] S. Gonuguntla, W. C. Lim, F. Y. Leong, C. K. Ao, C. Liu, S. Soh, *Sci. Adv.* **2021**, *7*, eabe5698.
[13] S. Ma, X. Li, S. Huang, J. Hu, H. Yu, *Angew. Chem. Int. Ed.* **2019**, *58*, 2655.
[14] R. Ajdary, B. L. Tardy, B. D. Mattos, L. Bai, O. J. Rojas, *Adv. Mater.* **2021**, *33*, 2001085.
[15] Z. Xiong, C. Zheng, F. Jin, R. Wei, Y. Zhao, X. Gao, Y. Xia, X. Dong, M. Zheng, X. Duan, *Sens. Actuators, B* **2018**, *274*, 541.
[16] C. Zheng, F. Jin, Y. Zhao, M. Zheng, J. Liu, X. Dong, Z. Xiong, Y. Xia, X. Duan, *Sens. Actuators, B* **2020**, *304*, 127345.
[17] Q. Chen, L. Han, J. Ren, L. Rong, P. Cao, R. C. Advincula, *ACS Appl. Mater. Interfaces* **2020**, *12*, 50052.
[18] P. Rastogi, B. Kandasubramanian, *Chem. Eng. J.* **2019**, *366*, 264.
[19] G. F. Hu, A. R. Damanpack, M. Bodaghi, W. H. Liao, *Smart Mater. Struct.* **2017**, *26*, 125023.
[20] M. Kang, Y. Pyo, J. y. Jang, Y. Park, Y.-H. Son, M. Choi, J. w. Ha, Y.-W. Chang, C. S. Lee, *Sens. Actuators, A* **2018**, *283*, 187.
[21] Q. Ge, H. J. Qi, M. L. Dunn, *Appl. Phys. Lett.* **2013**, *103*, 131901.
[22] H. Zhu, B. Xu, Y. Wang, X. Pan, Z. Qu, Y. Mei, *Sci. Robot.* **2021**, *6*, eabe7925.
[23] L. Feng, W. Shi, Q. Chen, H. Cheng, J. Bao, C. Jiang, W. Zhao, C. Zhao, *Adv. Healthcare Mater.* **2021**, *10*, 2100784.
[24] A. Sydney Gladman, E. A. Matsumoto, R. G. Nuzzo, L. Mahadevan, J. A. Lewis, *Nat. Mater.* **2016**, *15*, 413.
[25] Z. Ding, C. Yuan, X. Peng, T. Wang, H. J. Qi, M. L. Dunn, *Sci. Adv.* **2017**, *3*, e1602890.
[26] R. Sachse, A. Westermeier, M. Mylo, J. Nadasdi, M. Bischoff, T. Speck, S. Poppinga, *Proc. Natl. Acad. Sci. USA* **2020**, *117*, 16035.
[27] M. J. Jaffe, *Plant Physiol.* **1973**, *51*, 17.
[28] J. C. Athas, C. P. Nguyen, B. C. Zarket, A. Gargava, Z. Nie, S. R. Raghavan, *ACS Appl. Mater. Interfaces* **2016**, *8*, 19066.
[29] D. Zhang, Y. Zhong, Y. Wu, X. Zhang, M. D. Dickey, J. Yang, *Compos. Sci. Technol.* **2021**, *216*, 109066.
[30] R. R. Kohlmeyer, J. Chen, *Angew. Chem., Int. Ed.* **2013**, *52*, 9234.
[31] B. Han, Y.-L. Zhang, L. Zhu, Y. Li, Z.-C. Ma, Y.-Q. Liu, X.-L. Zhang, X.-W. Cao, Q.-D. Chen, C.-W. Qiu, H.-B. Sun, *Adv. Mater.* **2019**, *31*, 1806386.
[32] O. M. Wani, H. Zeng, A. Priimagi, *Nat. Commun.* **2017**, *8*, 15546.
[33] W. Fan, C. Shan, H. Guo, J. Sang, R. Wang, R. Zheng, K. Sui, Z. Nie, *Sci. Adv.* **2019**, *5*, eaav7174.
[34] M. del Pozo, C. Delaney, C. W. M. Bastiaansen, D. Diamond, A. P. H. J. Schenning, L. Florea, *ACS Nano* **2020**, *14*, 9832.
[35] Z.-C. Ma, Y.-L. Zhang, B. Han, X.-Y. Hu, C.-H. Li, Q.-D. Chen, H.-B. Sun, *Nat. Commun.* **2020**, *11*, 4536.
[36] H. Ceylan, N. O. Dogan, I. C. Yasa, M. N. Musaoglu, Z. U. Kulali, M. Sitti, *Sci. Adv.* **2021**, *7*, eabh0273.
[37] X. Liu, X. Pan, M. G. Debije, J. P. A. Heuts, D. J. Mulder, A. P. H. J. , Schenning, *Soft Matter* **2020**, *16*, 4908.
[38] M. del Pozo, C. Delaney, M. Pilz da Cunha, M. G. Debije, L. Florea, A. P. H. J. Schenning, *Small Struct.* **2022**, *3*, 2100158.
[39] W. Lei, G. Hou, M. Liu, Q. Rong, Y. Xu, Y. Tian, L. Jiang, *Sci. Adv.* **2018**, *4*, eaau8767.
[40] M. Omar, B. Sun, S. H. Kang, *Sci. Robot.* **2021**, *6*, eabh1560.
[41] D. D. Jin, Q. Y. Chen, T. Y. Huang, J. Y. Huang, L. Zhang, *Mater. Today* **2020**, *32*, 19.
[42] Y. Pan, L. H. Lee, Z. Yang, S. U. Hassan, H. C. Shum, *Nanoscale* **2021**, *13*, 18967.
[43] T. Zırıh, N. Orakdogen, *Eur. Polym. J.* **2016**, *75*, 371.
[44] H. Yu, H. Ding, Q. Zhang, Z. Gu, M. Gu, *Light: Adv. Manuf.* **2020**, *2*, 31.
[45] J. B. Mueller, J. Fischer, F. Mayer, M. Kadic, M. Wegener, *Adv. Mater.* **2014**, *26*, 6566.
[46] W. Gao, H. Chao, Y. C. Zheng, W. C. Zhang, M. L. Zheng, *ACS Appl. Mater. Interfaces* **2021**, *13*, 27796.
[47] Y. Hu, Z. Wang, D. Jin, C. Zhang, R. Sun, Z. Li, K. Hu, J. Ni, Z. Cai, D. Pan, X. Wang, W. Zhu, J. Li, D. Wu, L. Zhang, J. Chu, *Adv. Funct. Mater.* **2020**, *30*, 1907377.
[48] M. Hippler, E. Blasco, J. Qu, M. Tanaka, C. Barner-Kowollik, M. Wegener, M. Bastmeyer, *Nat. Commun.* **2019**, *10*, 232.
[49] Y. Lin, C. Zhang, W. Tang, Z. Jiao, J. Wang, W. Wang, Y. Zhong, P. Zhu, Y. Hu, H. Yang, J. Zou, *Adv. Sci.* **2021**, *8*, 2102539.
[50] S. Armon, E. Efrati, R. Kupferman, E. Sharon, *Science* **2011**, *333*, 1726.